Seismic Behavior and Shaking Direction Influence on Adobe Wall Structures Reinforced with Geogrid

Stefano Bossio,[a] Marcial Blondet,[b] M.EERI, and Satwant Rihal,[c] M.EERI

The aim of this work was to assess and validate the construction technology proposed in the manual published by the Pontificia Universidad Católica del Perú (PUCP), *Building Hygienic and Earthquake-Resistant Adobe Houses Using Geomesh Reinforcement*. In order to validate the proposed technology, two full-scale adobe wall house models were built and subjected to dynamic tests on the PUCP's unidirectional shaking table. Geogrid was used as reinforcement for the adobe walls. One of the models was aligned with the direction of shaking, so that its longitudinal walls were subjected to in-plane forces and its transverse walls to out-of-plane forces. The other model was turned 45° with respect to the direction of shaking in order to have all the walls subjected to both in-plane and out-of-plane forces. The results of both tests were also compared to those obtained during previous tests of an unreinforced adobe model. [DOI: 10.1193/1.4000096]

INTRODUCTION

It is well known that vernacular earthen construction (adobe, tapial) is extremely vulnerable to earthquakes. Every time an earthquake occurs in areas where this type of construction is common, there is widespread destruction, significant economic loss, and regrettable injuries and deaths. Researchers at the Catholic University of Peru (PUCP) have been working since the 1970s to develop and implement simple and cost-effective reinforcement solutions to reduce the vulnerability of adobe structures (Vargas et al. 2005). In recent years, several testing programs at the PUCP's Structures Laboratory have demonstrated that it is possible to improve the seismic behavior of adobe structures using geogrid (or geomesh) reinforcement (Blondet et al. 2005, 2006, 2008b, Torrealva and Acero 2005, Peralta 2009). During cyclic static and seismic simulation tests, adobe structures reinforced with geogrid maintained their integrity, providing enhanced resistance and deformation capacity. This technology has also been used recently to repair and retrofit existing adobe buildings (Zapata and Torrealva 2010).

The earthquake of 15 August 2007 caused extensive damage in the Peruvian regions of Lima, Ica, and Huancavelica. Almost 600 people died, and more than 90,000 buildings were destroyed (INDECI 2009). Few confined masonry or reinforced-concrete buildings suffered significant damage. Most of the structures that collapsed or suffered extensive damage were

[a] University College London, Gower Street, London, WC1E 6BT
[b] Catholic University of Peru, Avenida Universitaria 1801, Lima 32, Peru
[c] California Polytechnic State University, San Luis Obispo, CA 93407

Earthquake Spectra, Volume 29, No. 1, pages 59–84, February 2013;

made with adobe (Blondet et al. 2008c). In response to this devastating earthquake, PUCP decided to carry out a training and reconstruction project in the affected areas using this new adobe house construction technology (Blondet et al. 2008a). As part of the technology transfer implementation plan PUCP distributed the manual *Building Hygienic and Earthquake-Resistant Adobe Houses Using Geomesh Reinforcement* (Vargas et al. 2007). The manual is still being used to build new adobe houses in the areas affected by the Pisco earthquake.

This paper describes the results of a shaking table test program developed to assess and validate the construction system as published by PUCP and as put into practice after the 2007 Peru earthquake.

PROJECT DESCRIPTION

The aim of this project was to validate the reinforced-adobe construction system described in the manual published and distributed by PUCP (Vargas et al. 2007) after the 15 August 2007 earthquake in order to advance earthquake-resistant adobe house construction in seismic areas. For this purpose, two full-scale adobe house models with geogrid reinforcement were tested at the unidirectional shaking table of the PUCP's Structures Laboratory. The first reinforced model, called M1, was identical to an unreinforced adobe house model (M0) tested at the shaking table during a previous project (Blondet et al. 2006). Model M0 represented an unreinforced traditional adobe house, similar to those that have collapsed or suffered significant damage during past earthquakes. According to the Peruvian adobe code requirements (RNE 2006), although its adobe walls have adequate strength, this model would have required special seismic reinforcement due to the large wall slenderness. The geogrid-reinforced models M1 and M2 satisfy recently approved design requirements in the Peruvian adobe code (Torrealva 2009).

Shake table excitation for both M0 and M1 was in the longitudinal direction of the models (parallel to the east and west walls). Therefore, the east and west walls were subjected to in-plane seismic loads and the transverse (north and south) walls were subjected to out-of-plane loads. The second reinforced model (M2) was tested by placing it at 45° with respect to the shaking table movement. In this case, all walls were subjected to both in-plane and out-of-plane seismic loads.

The specific objective of the project was to assess the effectiveness of the geogrid reinforcement to provide the adobe walls the capacity to withstand seismic loads. This was done by comparing the dynamic behavior and performance of the three models tested. Of particular interest were the evaluation of the increase in strength and stiffness provided by the geogrid to the adobe walls, and the assessment of the influence of the orientation of the unidirectional ground shaking on the response of the reinforced walls.

MODEL DESCRIPTION AND CONSTRUCTION

Models M1 and M2 were reinforced with Tensar BX4100 geogrid (Tensar 2009). They were built with the configuration shown in Figures 1 and 2. Similar adobe housing models were tested in previous research projects (Torrealva and Acero 2005, Blondet et al. 2006). Each model consisted of four walls measuring 3.25 m (10.66 ft.) long, 0.25 m (0.82 ft.) wide, and variable height. Adobe bricks used were 250 mm (10 in.) × 250 mm (10 in.) × 70 mm (2.8 in.) (L × W × H) in size. They were made from soil, straw, and coarse sand in the

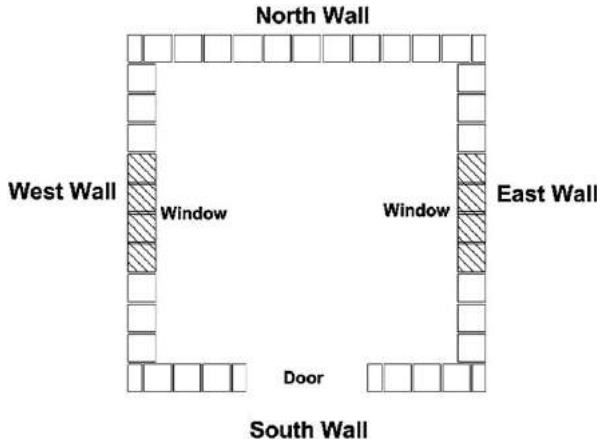

Figure 1. Model configuration of ground plan.

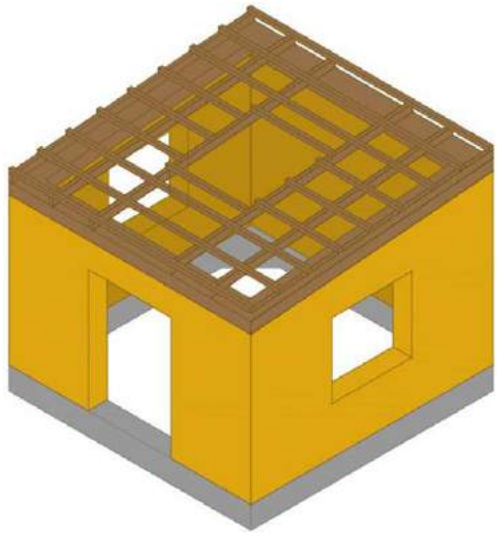

Figure 2. Isometric view of the model.

proportional volume of 5:1:1. Vertical and horizontal joints were 20 mm (0.8 in.) wide and were filled with mud mortar. The volume proportion of the mud mortar mixture was 3:1:1 (soil:straw:coarse sand). The minimum allowable compressive strength of this type of adobe masonry is 200 kN/m^2 and the minimum allowable shear strength is 25 kN/m^2 according to Peruvian national standards (RNE 2006).

East and west walls were identical and had a central window opening. The door opening was in the south (front) wall, whereas in the north (back) wall there were no openings. The

roof had a slope of 8 percent in the north-south direction The models were built over a reinforced-concrete square ring beam 3.25 m (10.66 ft.) long each side and 0.30 m (1 ft.) by 0.30 m (1 ft.) cross section, which simulated a rigid house foundation. Furthermore, the ring beam was used to attach the model to the shaking table and as a support during transportation from the building area to the test site. Figure 3 provides elevation views of all four walls.

Door and window lintels consisted of pieces of cane placed in three layers and tied up every 0.40 m (1.31 ft.) with #16 wire (Figure 4). Placing these "flexible" lintels was intended to avoid the large amount of cracks that usually appear through the wall-lintel corners during shaking, absorbing the tensile stresses that concentrate in these areas. A wooden collar beam was placed on top of the walls to provide some load transfer and displacement compatibility at wall intersections. The roof system behaved therefore as a semi-rigid diaphragm.

The roof was placed upon the wooden collar beam. It consisted of 2 × 6-in. wooden beams placed every 0.55 m (1.80 ft.) in the north-south direction. Strips of wood measuring 1½ × 2 in. were placed every 0.40 m (1.31 ft.) perpendicular to the north-south beams, as shown in Figure 5.

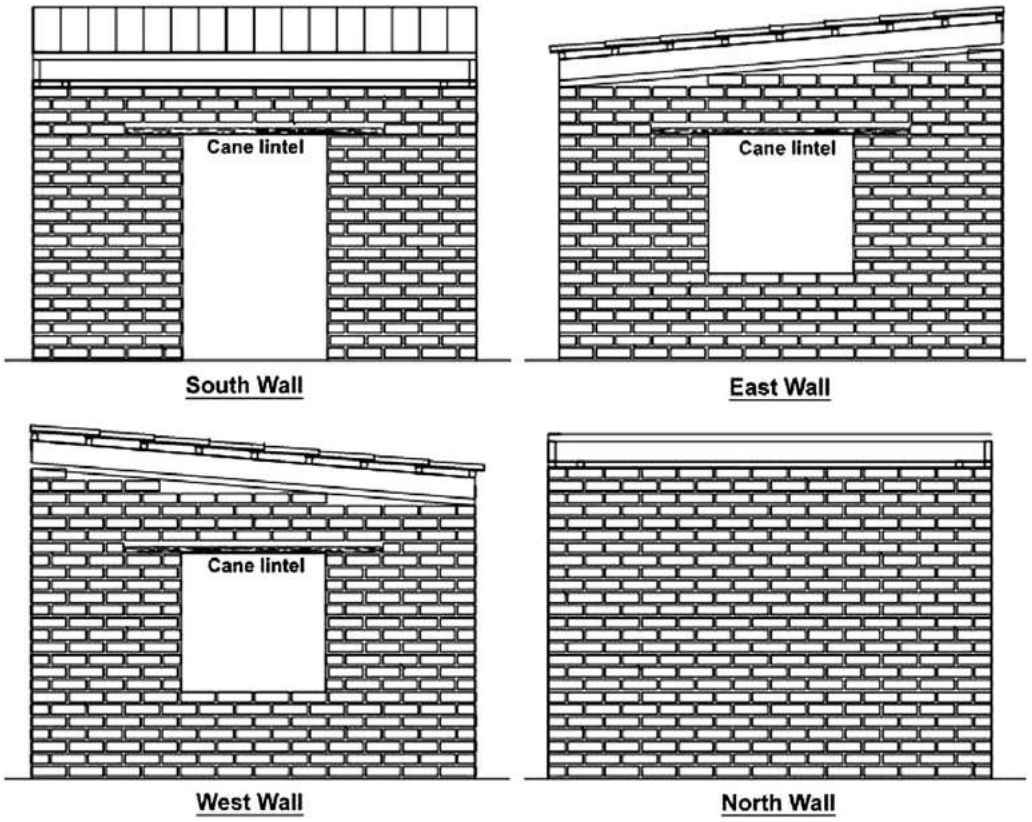

Figure 3. Elevation of walls: (a) south wall; (b) east wall; (c) west wall; (d) north wall.

Figure 4. Cane lintel.

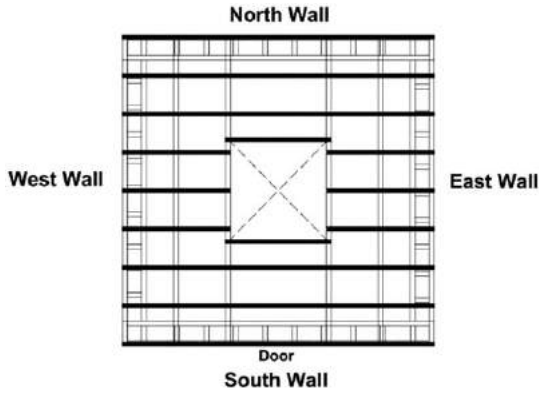

Figure 5. Roof framing.

The Tensar BX4100 geogrid (Tensar 2009) used in this project is available in Peru at a cost of U.S. $1.15/m^2. The total amount of geogrid per model was 95.14 m^2 (1,024 ft.^{2}) with a cost of U.S. $109.40. The geogrid is conveniently sold in rolls of 3 or 4 m (9.8 or 13.1 ft.) in width and 75 m (246 ft.) in length, as can be seen in Figure 6. Tensar offers other types of geogrid, such as the BX1100 and BX1200, which have been used in previous projects (Torrealva and Acero 2005; Blondet et al. 2006), with a cost of U.S. $1.45/m^2 and U.S. $3.45/m^2, respectively. Although the tensile strength of the BX4100 is the lowest among these geogrids, its use was based on economic criteria. Table 1 shows a comparison of mechanical properties of the above-mentioned geogrids. Tensile strength tests were carried out to verify the nominal tensile strengths specified by the supplier. All strength values measured were higher than the ones provided by the supplier, which were considered reliable (Bossio 2010).

During the setup of the adobe walls, plastic strips were placed between adobes (Figures 7 and 8) as a means of attaching the geogrid to the walls. These mooring points were composed

Figure 6. Geogrid roll.

of four plastic strips of 0.60 m (2 ft.) long each and placed 0.25 m (10 in.) apart horizontally and every three adobe layers vertically. Eight pieces of geogrid were cut corresponding to each face of the model. After each piece was placed upon the face of the wall, the plastic strips were passed through the geogrid holes and tied, fastening the reinforcement to the model (Figure 9).

A piece of geogrid was wrapped around the foundation ring to simulate the anchorage of geogrid inside the plinth as specified in the manual (Figure 10). The lower parts of the geogrids, which wrap the walls, were tied to the foundation geogrids with plastic thread strips. On the upper part of the walls, the vertical geogrids of opposite faces were tied with plastic strips and fastened to the wooden collar beams. All geogrid overlaps were 0.40 m and tied with plastic strips (Figure 11).

Table 1. Mechanical properties of geogrids (Tensar 2009)

		BX1100		BX1200		BX4100	
Property	Units	MD	XMD	MD	XMD	MD	XMD
Aperture dimensions	mm (in)	25 (1.0)	33 (1.3)	25 (1.0)	33 (1.3)	33 (1.3)	33 (1.3)
Minimum rib thickness	mm (in)	0.76 (0.03)	0.76 (0.03)	1.27 (0.05)	1.27 (0.05)	0.76 (0.03)	0.76 (0.03)
Tensile strength @ 2% strain	kN/m (lb/ft)	4.10 (280)	6.60 (450)	6.00 (410)	9.00 (620)	4.00 (270)	5.50 (380)
Tensile strength @ 5% strain	kN/m (lb/ft)	8.50 (580)	13.40 (920)	11.80 (810)	8.00 (550)	8.00 (550)	10.50 (720)
Ultimate tensile strength	kN/m (lb/ft)	12.40 (850)	19.00 (1,300)	19.20 (1,310)	28.80 (1,970)	12.80 (880)	13.50 (920)

MD: Main direction; XMD: Cross main direction

Figure 7. Placing plastic strips.

Figure 8. Setting adobe bricks.

Figure 9. Placing and tying the piece of geogrid.

Figure 10 Foundation geogrid.

Figure 11 Tying the geogrid overlaps.

Figure 12. Preparing the mortar.

Figure 13. Placing the first mud plaster layer.

The wall finish was placed in two phases. A first layer of mud plaster 10 mm (0.4 in.) thick was placed using a mixture with a proportion of 3:2:1 (soil:straw:coarse sand). Figures 12 and 13 show this process. Then a second layer of mud plaster 15 mm (0.6 in.) thick of the same mixture was placed (Figure 14). Finally, two days after the second layer was finished, the cracks caused by drying shrinkage of the mud plaster were repaired by applying a fluid mixture of soil and fine sand in the proportional volume of 1:1 to the wall's surface, using a paintbrush. The model was then left to dry for one month before the test (Figure 15).

In contrast to the reinforced models M1 and M2 that were completely plastered, only the east wall was plastered in model M0. Furthermore, the wooden collar beam that ties all walls was not placed in model M0. The roof was directly placed upon strips of wood fitted on the

Figure 14. Placing the second plaster layer.

Figure 15. Finished model.

walls in order to simulate the typical construction in unreinforced adobe houses in the rural areas of Peru.

TEST PROTOCOL AND MODEL INSTRUMENTATION

The shaking table input signal used in these tests was obtained from an accelerogram recorded in Lima during the 31 May 1970 earthquake that occurred near the central coast of Peru. The east-west component was subjected to digital filtering and double integration to obtain a displacement record that was used as the command signal for the shaking table. Figure 16 shows the 30-second displacement command signal normalized to 1 mm (0.04 in.) of peak amplitude.

Each test consisted of three phases, defined by the peak command displacement for the shaking table platform. The first phase had a maximum displacement of 30 mm (1.2 in.), the second phase a maximum of 80 mm (3.2 in.), and the third phase a maximum of 130 mm (5.2 in.). The expected peak table accelerations, based on previous similar tests, were approximately 0.30 g, 0.70 g, and 1.20 g, respectively.

No equivalence has been established between the PUCP shaking table motion and a specific earthquake ground motion. This is because the unidirectional shaking table can

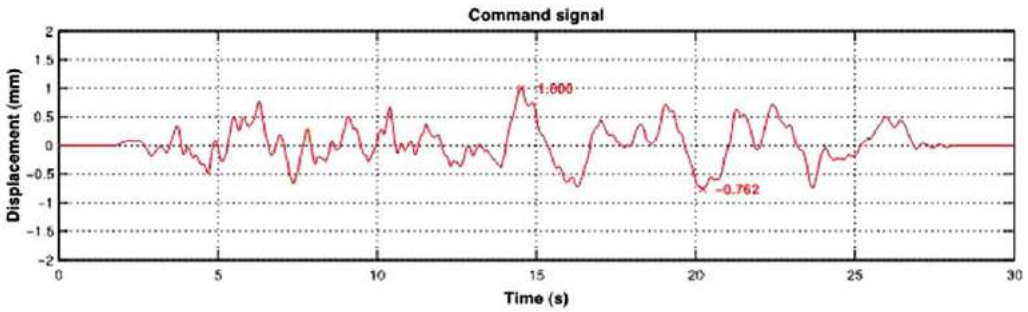

Figure 16. Command signal with maximum displacement normalized to 1 mm.

reproduce only one component of the ground shaking, thus inducing lower stresses than those that would have occurred in the field, where the ground shakes in all directions simultaneously. For instance, in the Pisco area, where most of the adobe houses collapsed or suffered significant damage during the 2007 earthquake, the modified Mercalli intensity was between VII and VIII (USGS 2007). The estimated peak ground acceleration within these intensity levels is 0.34 g. Most of the adobe houses were also destroyed during the Nazca, Peru, earthquake of 1996 in the areas where the MM intensity was between VII and VIII (EERI 1996). Similarly, in the Atico, Peru, 2001 earthquake, the ground acceleration was lower than 0.30 g (Fierro 2001). Therefore, although Peruvian traditional unreinforced adobe houses collapse at ground acceleration levels of about 0.30 g, similar structures subjected to unidirectional shaking table motions collapse at acceleration levels above 0.60 g. To date this effect has not been studied thoroughly for adobe construction, and therefore unidirectional shaking table tests are used mainly to compare the relative seismic performance of similar structures with different reinforcement configurations, such as in this study.

It is expected that the comparison of the seismic response of model M1 (where the longitudinal walls are subjected to in-plane forces only and the transverse walls to out-of-plane forces only) to that of model M2 (where all four walls are subjected simultaneously to both in-plane and out-of-plane forces) will be a first step towards the study and understanding of the effects of multidirectional shaking on the dynamic behavior of adobe structures.

Nevertheless, from the observed damage of adobe houses during past earthquakes, and in numerous shaking table tests carried out with the same command signal, the three test phases applied in this study may be considered analogous to mild, moderate, and strong earthquakes. It is expected that a mild earthquake would cause minor cracking on the walls of a typical unreinforced adobe house; a moderate earthquake would cause significant cracking, especially in the intersections of the adobe walls; and a strong earthquake would cause total or partial collapse of the structure.

Before each of the three test phases was carried out and at the end of the test, the model was subjected to a sequence of rectangular displacement pulses (Figure 17) that induced free vibration motion. This was done to estimate the vibration period and equivalent viscous damping of the models.

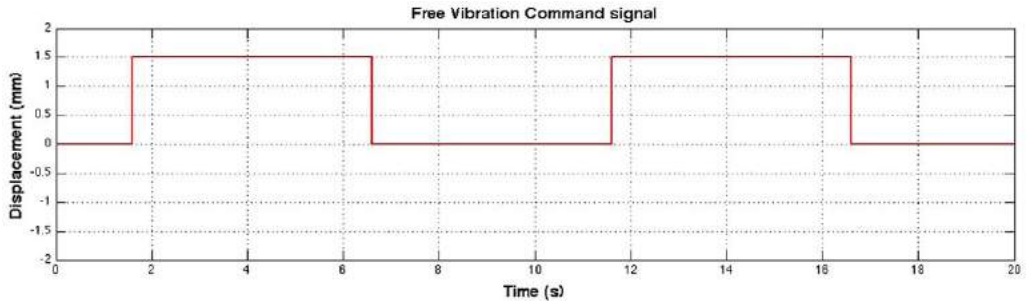

Figure 17. Free vibration command signal.

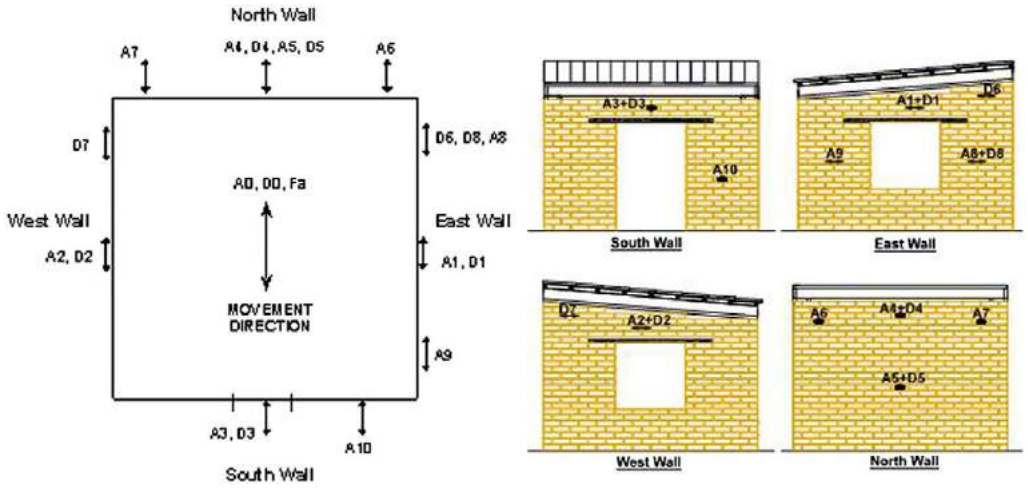

Figure 18. Ground plan and elevation distribution of instruments in models M0 and M1.

The instrumentation in models M0 and M1 was based on previous projects carried out at PUCP (Torrealva and Acero 2005; Blondet et al. 2006). Ten accelerometers were placed on the model to record absolute accelerations (referred as A# in Figure 18) and eight linear variable differential transformers (LVDTs) were used to record absolute displacements (referred as D# in Figure 18). Additionally, one LVDT, one accelerometer, and one force sensor were located at the platform actuator and recorded test data as well.

It was necessary to modify the instrumentation layout in model M2 to record response data properly due to the change of orientation of the model. Twelve accelerometers and

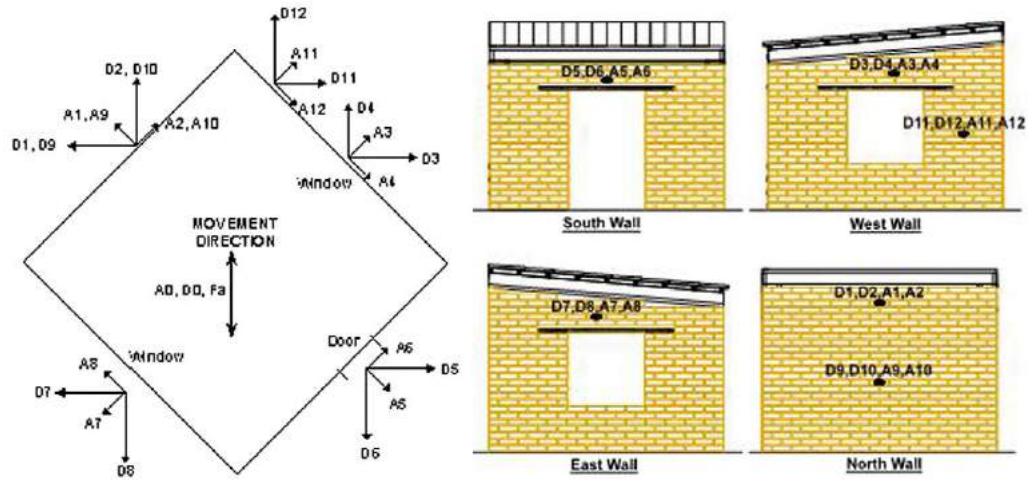

Figure 19. Ground plan and elevation distribution of instruments in model M2.

twelve LVDTs (referred as A# and D#, respectively, in Figure 19) were placed on the model. The same instruments were located at the table platform as in the previous models.

UNREINFORCED MODEL M0 TEST

The unreinforced adobe model was tested in a previous project (Blondet et al. 2006), where shaking table tests were carried out using the same test parameters. Results from this test were used as a reference and for comparison with the results from the reinforced models. Figure 20 shows the state of this model before the test.

During the first phase, there was no damage in the model (Figure 21a). During the second phase, the model suffered serious damage. Large diagonal cracks occurred in the east and west walls due to shear forces, and vertical cracks due to out-of-plane forces occurred on the north and south walls (Figure 21b). The difference between the east wall (plastered) and the west wall (unplastered) was noticeable. While the first wall was barely damaged, the second wall was severely affected. At the end of this phase, all LVDTs were removed from the model to prevent them from being damaged due to the imminent collapse of the structure. Thus, no displacements were recorded in the following test phase. During the third phase, the model suffered a partial collapse: North and south walls collapsed due to out-of-plane failure. Although east and west walls remained standing, they suffered significant diagonal cracking and some adobe bricks broke into pieces. This damage pattern is typical of contemporary vernacular adobe houses in many countries, which are built to imitate the architectural features of clay brick masonry houses: They are irregular in plan and elevation, do not have seismic reinforcement, and their walls have large window and door openings. When an earthquake occurs, the out-of-plane seismic forces produce large vertical cracks at the corners, and in-plane shear forces produce diagonal cracks in the walls. The walls are thus broken in large independent pieces, which fall down, causing in turn the collapse of the roof (Blondet and Villa Garcia 2004). In this case, due to the unidirectional shaking in the longitudinal (north-south) direction, the east and west walls were not subjected to out-of-plane forces and remained standing, barely supporting the roof with the total integrity of the model almost lost (Figures 21c and 21d). This test

Figure 20. Unreinforced model—M0.

Figure 21. Damage in model M0**.**

underscores the importance of a collar beam in preventing or at least delaying the out-of-plane collapse of the adobe walls due to strong seismic shaking.

REINFORCED MODEL M1 TEST

This model was fully reinforced with Tensar BX4100 geogrid. East and west walls of the model were parallel to the movement of the shaking table (Figure 22).

During the first phase, tiny cracks appeared in the corner of the window openings and in the inside corners of the walls (Figure 23a). These cracks were only in the mud plaster. There was no structural damage in the model. In the second phase these cracks grew significantly and slight structural damage was observed (Figure 23b). During the third phase, larger relative displacements between walls were observed. In the areas where maximum shear and out-of-plane forces occurred, the plaster fell from the wall (Figure 23c). After the test was finished, the plaster was removed and it was discovered that the geogrid was torn in the regions near the window corners, due to stress concentrations at these locations. Most of the geogrid damage occurred near the bottom corner of the west wall, where large diagonal cracks also appeared (Figure 23d). In conclusion, moderate damage was observed in the model, and the integrity of the structure was maintained.

Figure 22. Reinforced model—M1.

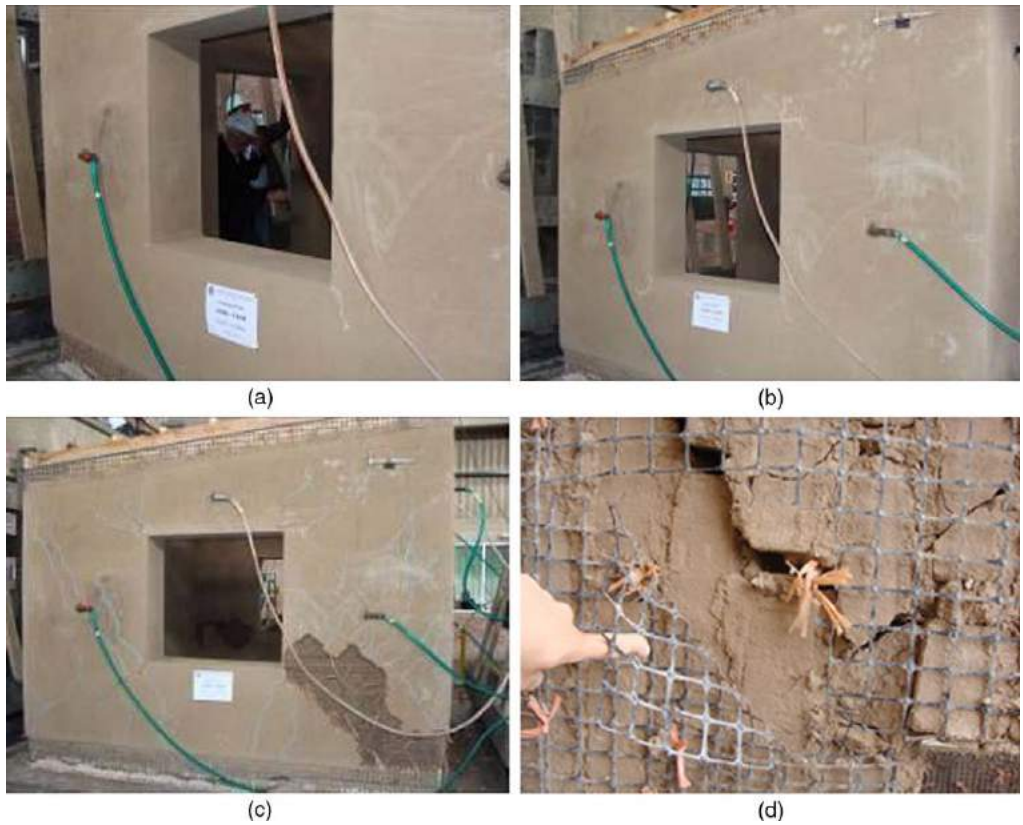

Figure 23. Damage in M1 model: (a) post-phase 1; (b) post-phase 2; (c) post-phase 3; (d) geogrid failure.

Figure 24. Reinforced model—M2.

REINFORCED MODEL M2 TEST

This model was fully reinforced with Tensar BX4100 geogrid as well. The model was rotated 45° with respect to the shaking table movement (Figure 24).

No damages were noticed after the first test phase (Figure 25a). During the second phase, small cracks in the mud plaster were observed in the corners of the windows and door openings (Figure 25b). No structural damage was observed during this phase. During the third phase, diagonal cracks occurred in the east and west walls due to shear and out-of-plane forces (Figure 25c). However, the model slid approximately 20 mm from its base during this phase (Figure 25d). Only slight structural damage—with cracks less than 20 mm in width—was observed in the model at the end of the test.

COMPARISON OF RESULTS

Special emphasis was placed on comparing the results of the unreinforced model to the reinforced models in order to evaluate the contribution of the geogrid reinforcement technology. In addition, it was of interest to evaluate the influence on the seismic behavior of changing the orientation of the model relative to the shaking direction.

After comparing the seismic behavior of the models and classifying the damage levels, it was evident that the geogrid reinforcement technology reduced the damages significantly from a nearly collapse state in model M0 to a moderate damage state in model M1. In some corners of the windows and door openings, the geogrid was found to be torn up, which demonstrates that the reinforcement worked properly, confining the walls and withstanding tensile stresses. Table 2 shows a comparison of the seismic behavior of the models at each phase of the test.

Plaster separation and wall cracking that does not go through the width of the wall is considered slight damage. The presence of larger cracks across the width of the wall, usually

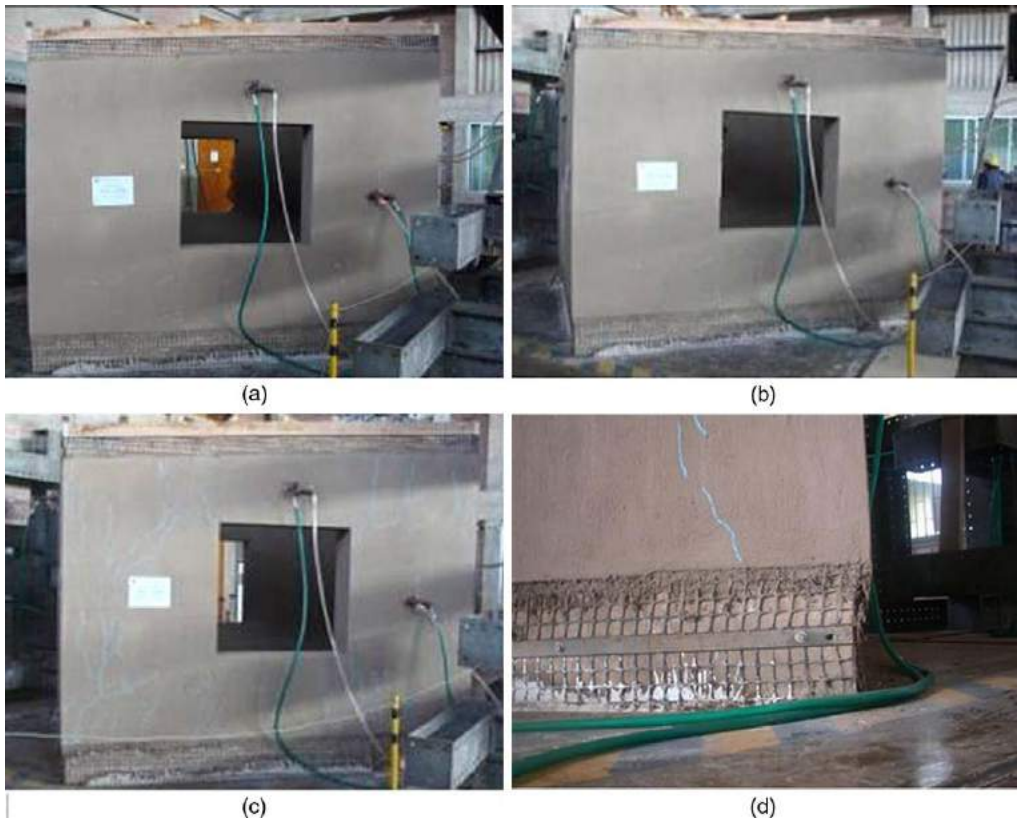

Figure 25. Damage in model M2: (a) Post-phase 1; (b) post-phase 2; (c) post-phase 3; (d) post-phase 3.

stepwise within the mortar-block interface or near wall openings and corners but that do not cause the separation of the wall into large pieces, is considered moderate damage. Wall cracking that causes separation of the wall in large pieces, usually followed by partial collapse, is considered serious damage.

In general, model M2 suffered less damage than model M1. Although this difference was clearly observed during the tests, the imposed displacements of the shaking table could have

Table 2. Seismic behavior of the models

Maximum displacement D_0 (mm)	M0	M1	M2(*)
30	No damage	No damage	No damage
80	Serious damage	Slight damage	No damage
130	Partial collapse	Moderate damage	Slight damage

*In the direction of the walls the displacement of the platform was $D_0/\sqrt{2}$.

Table 3. Damping factors in free vibration tests

Description	Model	VL0	VL1	VL2	VL3
East wall	M0	8.6%	9.2%	13.8%	–
	M1	7.9%	11.5%	11.9%	16.0%
	M2	8.9%	10.1%	10.4%	11.1%
West wall	M0	7.0%	8.1%	8.5%	–
	M1	8.6%	9.9%	11.4%	17.1%
	M2	6.2%	6.6%	10.1%	10.2%
South wall	M0	8.4%	9.4%	9.4%	–
	M1	6.9%	10.7%	11.7%	14.7%
	M2	6.0%	8.3%	8.5%	8.8%
North wall	M0	11.2%	13.6%	13.9%	–
	M1	8.7%	8.3%	9.6%	12.7%
	M2	7.8%	8.3%	9.1%	9.2%

had an influence on these results. In model M2, all walls were subjected to both shear and out-of-plane stresses, but in the direction parallel to the walls the displacement of the platform was 70% of the maximum displacement of M1. This difference could not be avoided due to the limitation in the maximum allowed displacement of the table platform of 150 mm (6 in.).

The increase in damage in the models was also estimated from the increase of the damping factor measured during the free vibration tests carried out before phase 1 (VL0) and after each of the three phases of the dynamic tests (VL1, VL2, and VL3, respectively). Table 3 shows the damping factors obtained from the accelerometers located at the top center of each wall using the method of logarithmic decrement.

An increment of the damping factor values was observed in all four walls after each phase of the test. Values in models M1 and M2 almost doubled at the end of the test. However, a lower increment in these values occurred in model M2 as corroborated with the lower damages observed. On average, the increment of values in model M0 was greater than the ones in the reinforced models, although this could only be corroborated with the instruments up to phase 2.

Using the data from the sensor at the top center of the north wall that measured transverse displacements of the wall and the force sensor, lateral force versus relative displacement graphs for each model were obtained (Figure 26).

For models M0 and M1 this instrument was D4 (Figure 18). For model M2, the sum of the components of D1 and D2 (Figure 19) in the transverse direction of the wall was used. The damage in this wall was mostly due to out-of-plane bending, thus this instrument was taken as representative of this type of damage. The relative displacement (DR) was obtained using the following equation:

$$DR_{\#} = D_{\#} - D_0 \tag{1}$$

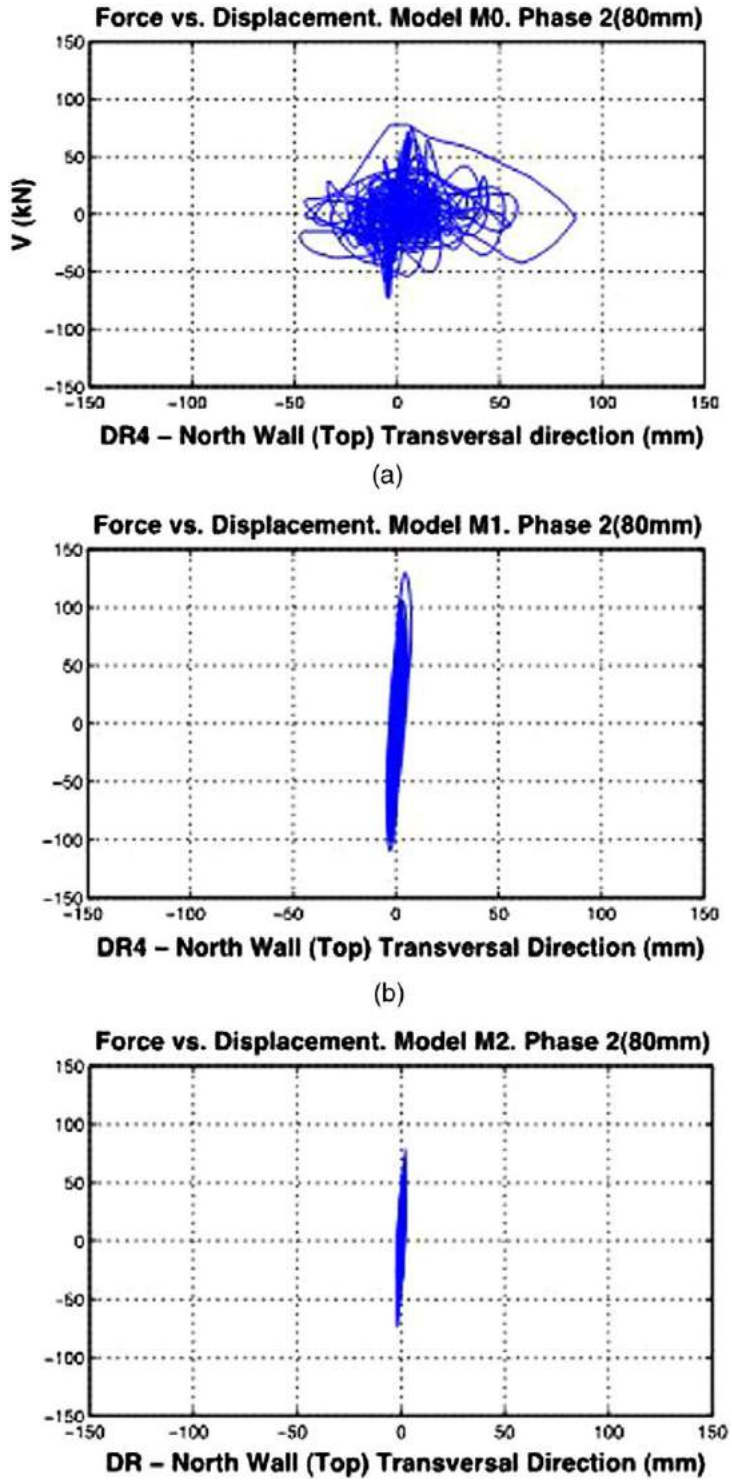

Figure 26. Lateral force vs. north wall top displacement, phase 2 (80 mm peak table displacement): (a) unreinforced model (M0); (b) Reinforced model (M1); (c)) reinforced model (M2).

where $DR_{\#}$ is the relative displacement of the instrument # (mm), $D_{\#}$ is the total displacement of the instrument # (mm), and D_0 is the table platform displacement (mm).

Data from the force sensor represented the amount of force needed to move the platform according to the command signal. In order to obtain the lateral force applied at the base of the model, this value had to be reduced by the inertial forces due to the platform and foundation ring masses. The lateral force V applied to the base of the whole structure was thus computed as:

$$V = F_a - (P_p + P_a) \times A_0 \tag{2}$$

where V is the lateral force applied at the base of the model (kN), F_a is the force applied to the platform (kN), P_p is the platform weight $= 176,58$ (kN), P_a is the foundation ring weight (depends on model) (kN), and A_0 is the acceleration at the table platform in terms of g.

The graphs in Figure 26 describe the performance of the north wall during phase 2 of testing. In model M2, the equation to obtain the lateral, in-plane force (i.e., the base force parallel to the north-south model axis) was changed due to the orientation of this model with respect to the direction of table motion. The lateral force applied to the model was obtained with Equation 3 below:

$$V_{M2} = V/\sqrt{2} \tag{3}$$

where V_{M2} is the lateral force component applied at the base of the model M2 (kN), and V is the total lateral force applied at the base of the model (kN).

Figure 26 shows that during phase 2 both reinforced models remained elastic, and thus undamaged, whereas unreinforced model M0 went beyond the elastic range, dissipated a significant amount of energy, and suffered major damage, almost reaching collapse state at the end of this phase.

Data from the accelerometers at the top of the north wall in phase 2 were compared in Figure 27 in order to observe the influence of the geogrid reinforcement. The bottom graph corresponds to the accelerometer located on the platform of the shaking table.

The accelerations recorded in the reinforced models were significantly lower than the ones recorded in model M0. Maximum accelerations in models M1 and M2 were 73% and 51% of those in model M0, respectively. Also, it is possible to note that for model M0 the dominant frequency of vibration at the end of the phase is significantly lower than at the beginning, which indicates loss of global stiffness due to damage in the wall.

It was of special interest to compare the graphs of lateral force versus relative displacement envelopes of the adobe walls. The procedure to obtain the envelope of a wall's behavior in a cyclic test (e.g., Torrealva 2009) was modified by the authors in order to apply it to a dynamic test. Data from the LVDTs at top center of the north and east walls were used to calculate relative displacements. In order to obtain the response envelopes, the total duration of each phase was divided into 12 intervals of 2.5 seconds each. For each interval, a graph of lateral force versus relative displacement was obtained. Then, the data points where

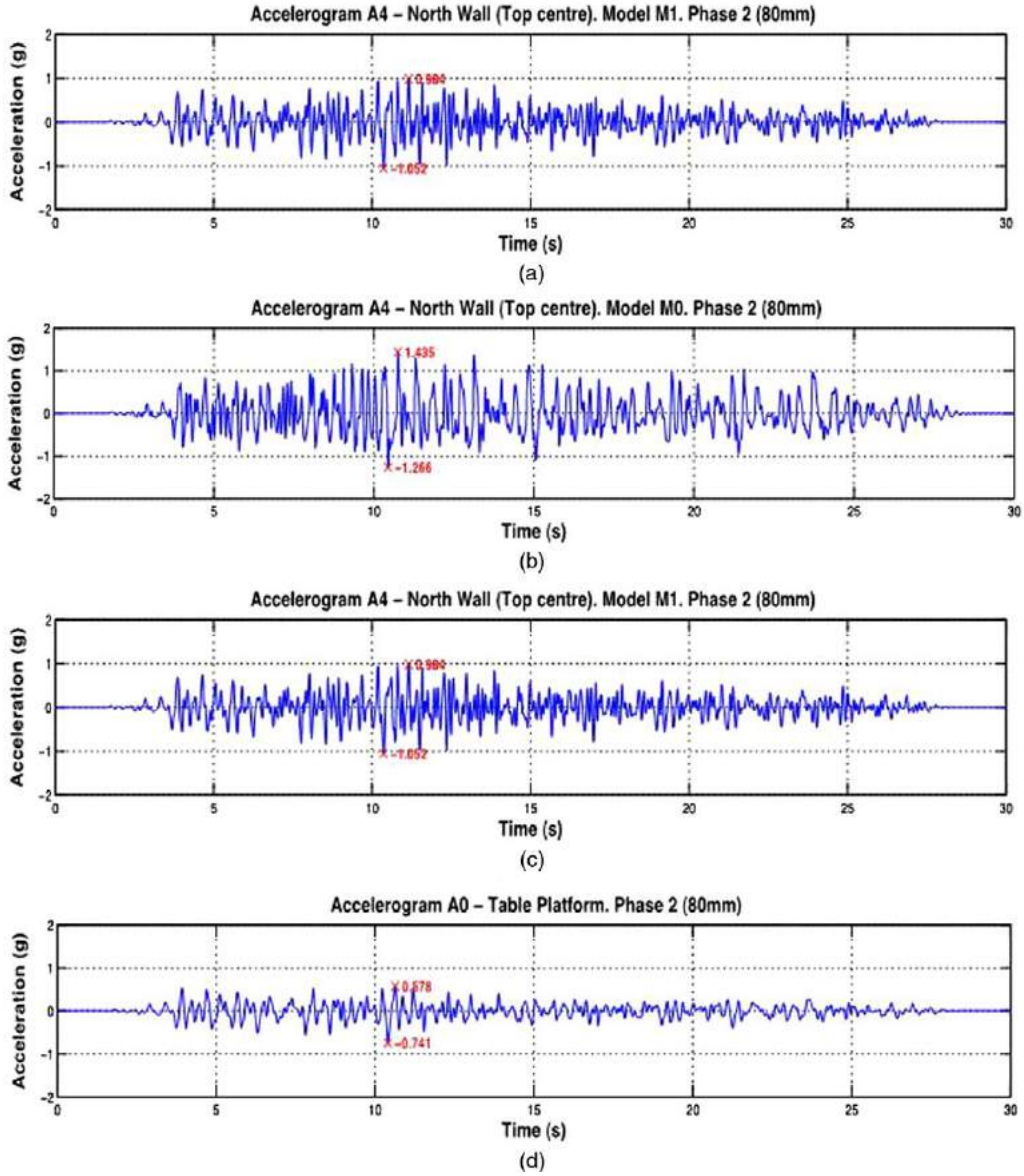

Figure 27. Recorded accelerations for phase 2—top north wall.

minimum and maximum displacements and forces occurred were identified and selected. Therefore, four points for each interval and 48 points for each phase were obtained. These data points were plotted on the first quadrant by taking absolute value of each ordinate, and the envelope of all points was generated. Lateral forces were divided by the mass of the whole structure so as to eliminate the influence of this variable in the graphs. The ordinates thus represent seismic coefficient or pseudoacceleration (base shear per unit mass). Markers

indicate where change of phase occurred. Figure 28 shows the envelopes for the west wall (subjected to in-plane forces in models M0 and M1) and Figure 29 for the north wall (subjected to out-of-plane forces in models M0 and M1).

A great difference is shown in Figure 28 between the envelope of model M1 (reinforced) and model M0 (unreinforced). Model M1 reached approximately 155% of the base shear force of model M0. Approximately 10% of this strength increase can be attributed to the extra 25 mm (1 in.)-thick mud plaster applied on each face of model M1 walls (600 mm total longitudinal wall thickness), whereas only the east wall was plastered in M0 (550 mm total longitudinal wall thickness). Therefore, the remaining strength increase was provided by the geogrid. The difference in elastic stiffness is also noticeable in Figure 28, where model M1 is significantly stiffer than M0. (A comparison of the average slopes of the lateral force versus relative displacement graphs shows that the lateral stiffness of M1 is twice that of M0.) It seems that the mud plaster placed on the walls of M1 was able to provide adequate confinement to the reinforcement, thus allowing for a good integration between the adobe and geogrid.

These results prove that the reinforcement technology provides a considerable enhancement in the seismic strength capacity of the adobe models. Moreover, large displacements and damages occurred in M0 during phase 2, whereas in the reinforced models these did not occur until phase 3. Furthermore, model M0 was nearly incapable of withstanding forces at the end of phase 2. The damage at this state was due to in-plane shear forces. Significant diagonal cracks appeared throughout the wall in one or two directions (X shape), reducing the wall section and ultimately leading to its collapse, as shown in Figure 21.

A large amount of displacement ductility, of about 8, was observed in model M1, which reached a maximum displacement of 83 mm (3.3 in.) with a reduction of the maximum lateral force of 50%. A lower displacement ductility of approximately 4.4 was observed in model M2 due to the lower input in the table platform, with a reduction of 10% of the maximum lateral force. The walls in these two models were still capable of dissipating energy at the end of the test.

Similar behavior was observed for the north wall, as shown in Figure 29. For the same amount of displacement, the walls in model M2 withstood lower lateral forces

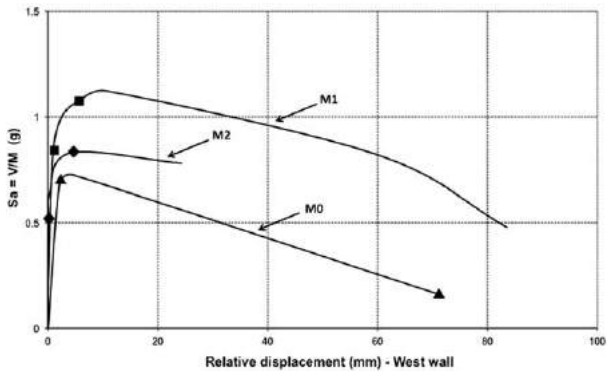

Figure 28. Lateral force vs. relative displacement envelope—west wall.

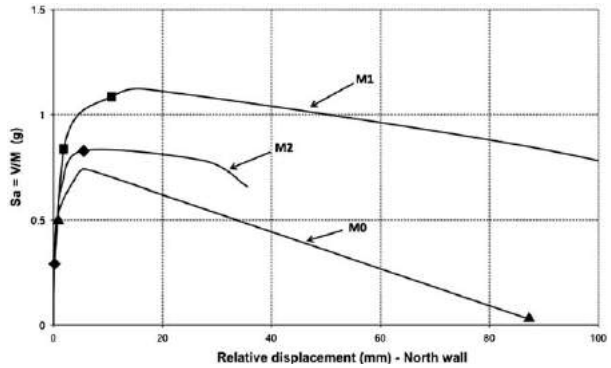

Figure 29. Lateral force vs. relative displacement envelope—north wall.

(approximately 74%) than those in model M1. This trend was observed up to phase 2. However, during phase 3 a sliding occurred at the base of model M2 (Figure 25d), thus not letting the walls reach their real strength capacity. No conclusion could be made for this phase. Nevertheless, from data of the first two phases of the tests, it was evident that the action of combined (and in-phase) forces in parallel and perpendicular direction to the walls reduced the amount of lateral force that the structure could withstand.

Finally, Table 4 presents peak values of relative displacement and base shear force calculated for the east and west walls. Angular distortion, computed as relative displacement divided by the height of the instrument, and average shear stress are also presented there.

It is interesting to note that, during phase 2, the average peak shear stress computed for model M0 was 41.6 kN/m^2. This value, slightly higher than the elastic shear strength of the unreinforced adobe walls (Figure 26a), is consistent with the shear strength of 41 kN/m^2 obtained during cyclic lateral testing of a full-scale unreinforced adobe wall (Blondet et al. 2005). The presence of the geogrid and the additional mud plaster increased this strength by 47%. Since only the east wall was plastered in model M0, the deformation of the unplastered west wall was almost five times larger than that of the east wall, where the mud plaster increased its thickness and thus its lateral stiffness and strength. Although both models M1 and M2 were clearly within their elastic range, due to the reduced input in its longitudinal direction, the response parameters estimated for model M2 are consistently lower than those of model M1.

During phase 3, the transverse walls of model M0 collapsed. Therefore, measurements taken during that phase are unreliable and are not shown on Table 4b. Behavior of models M1 and M2 was clearly beyond the elastic range. The negative slope of the force-displacement envelope indicates progressive stiffness and strength deterioration of both models due to spalling of the mud plaster, cracking of the adobe walls, and tearing of the geogrid in model M1. Sliding of model M2 over its concrete base most probably provided some isolation and prevented the development of larger shear forces in its longitudinal walls. As in the case of phase 2, response parameters estimated for model M2 are consistently lower than those of model M1.

Table 4. Summary of peak response of longitudinal walls during phases 2 and 3

(a) During phase 2 (D0 = 80 mm)

	West wall (peak values)		East wall (peak values)		Both walls (average values at peak force)		
Model	Relative displ. mm	Angular distortion %	Relative displ. mm	Angular distortion %	Shear force kN	Shear stress kN/m^2	Longitudinal table accel. g
M0	71.1	3.36%	15.0	0.71%	77.9	41.6	0.741
M1	5.2	0.24%	4.2	0.20%	130.2	61.3	0.721
M2	2.7	0.13%	1.7	0.08%	78.5	36.9	0.492

(b) During phase 3 (D0 = 130 mm)

	West wall (peak values)		East wall (peak values)		Both walls (average values at peak force)				
Model	Relative displ. mm	Angular distortion %	Relative displ. mm	Angular distortion %	Shear force kN	Shear stress kN/m^2	Relative displ. mm	Angular distortion %	Longitudinal table accel. g
M1	83.5	3.95%	64.5	3.05%	147.0	69.2	10.1	3.50%	1.121
M2	29.3	1.39%	33.1	1.57%	97.9	46.1	3.1	1.48%	1.076

CONCLUSIONS AND RECOMMENDATIONS

- The geogrid reinforcement proposed in the manual significantly reduces the seismic vulnerability of adobe wall structures, reducing the damage level and maintaining the structure's integrity even when subjected to large displacements and accelerations in the shaking table at the PUCP's Structures Laboratory. Further research that includes variations in the configuration of the models to simulate typical adobe structures built in different parts of Peru should be carried out in order to corroborate these results.
- The reinforcement technology demonstrated itself to be compatible with the deformation response of adobe structures and capable of developing ductile behavior when the structures are subjected to dynamic lateral forces.
- Model M2 was rotated 45° in order to obtain in-plane and out-of-plane responses in all walls so as to represent real lateral movement of a structure during an earthquake. Combined in-plane shear and out-of-plane stresses in adobe wall structures are shown to influence their seismic behavior, reducing the maximum shear force in the elastic phase that they could withstand when subjected to only one type of stress. Further experimental and analytical research is required to study and understand the effect of multidirectional seismic shaking on the behavior of adobe walls.

- The dynamic performance of the proposed construction technology published in the manual *Building Hygienic and Earthquake-Resistant Adobe Houses Using Geomesh Reinforcement*, tested in the PUCP's shaking table, demonstrated that it allows the adobe wall structure to withstand movements associated with strong earthquakes while suffering only moderate damage.

ACKNOWLEDGEMENTS

The authors are grateful to Luis Guzman-Barron, PUCP former rector, who provided funds for this project; to Professor Julio Vargas who co-directed the experimental phase; to engineer Felipe Montoya, who helped develop the final version of the paper; to the undergraduate and graduate students who helped during the tests; and to the Structures Lab personnel.

REFERENCES

Bossio, S., 2010. Evaluación del Comportamiento Sísmico e Influencia de la Dirección del Movimiento en Módulos de Adobe Reforzado con Geomalla, Tesis para optar el Título Profesional de Ingeniero Civil (Evaluation of the Seismic Behavior and Influence of Seismic Movement Direction on Adobe Modules Reinforced with Geogrid, Thesis to obtain the Civil Engineering Professional Diploma), Pontificia Universidad Católica del Perú, Lima.

Blondet, M., and Villa Garcia, G., 2004. Earthquake resistant earthen buildings?, *Proceedings, 13th World Conference on Earthquake Engineering*, Vancouver, B.C., Canada.

Blondet, M., Torrealva, D., Villa García, G., and Ginocchio F y Madueño, I., 2005. Using industrial materials for the construction of safe adobe houses in seismic areas, *EarthBuild2005 International Conference, University of Technology*, Sydney, Australia.

Blondet, M., Vargas, J., Velasquez, J., and Tarque, N., 2006. Seismic reinforcement of adobe houses using external polymer mesh, *Proceedings, First European Conference on Earthquake Engineering and Seismology*, Geneva, Switzerland.

Blondet, M., Vargas, J., Patron, P., Stanojevich, M., and Rubiños, A., 2008a. Human development approach for the construction of safe and healthy adobe houses in seismic areas, *Proceedings, 14th World Conference on Earthquake Engineering*, Beijing, China.

Blondet, M., Vargas, J., and Tarque, N., 2008b. Available low-cost technologies to improve the seismic performance of earthen houses in developing countries, *Proceedings, 14th World Conference on Earthquake Engineering*, Beijing, China.

Blondet, M., Vargas, J., and Tarque, N., 2008c. Observed behavior of earthen structures during the Pisco (Peru) earthquake of August 15, 2007, *Proceedings, 14th World Conference on Earthquake Engineering*, Beijing, China.

Fierro, E. 2001. Initial Report on 23 June 2001 Atico, Peru Earthquake—Part II, published in http://www.eeri.org/lfe/pdf/peru_arequipa_initial_reconnaissance_part2.pdf.

Earthquake Engineering Research Institute (EERI), 1997. Learning from earthquakes: The Nazca, Peru, earthquake of November 12, 1996, *Special Earthquake Report from the January 1997 Newsletter*.

Instituto Nacional de Defensa Civil (INDECI), 2009. *Lecciones Aprendidas del Sur—Sismo de Pisco 15 Agosto 2007* (Lessons Learned from the South—15 August 2007 Pisco Earthquake), Instituto Nacional de Defensa Civil, Lima, Peru, 232 pp.

Peralta, G., 2009. Resistencia a Flexión de Muros de Adobe Reforzados con Geomallas—Influencia del Tipo de Tarrajeo, Tesis para optar el Título Profesional de Ingeniero Civil (Flexural Strength of Adobe Walls Reinforced with Geogrid—Influence of the type of Plaster, Thesis to obtain the Civil Engineering Professional Diploma), Pontificia Universidad Católica del Perú, Lima, Peru.

Reglamento Nacional de Edificaciones (RNE), 2006. *Norma Técnica E.080 Adobe* (Technical Code E.080 Adobe), Lima, Peru.

Tensar International Corporation (Tensar), 2009. *Product Specification Tensar Biaxial Geogrid*, Tensar, Atlanta, GA, 13 pp.

Torrealva, D., 2009. *Diseño Sísmico de Muros de Adobe Reforzados con Geomalla* (Seismic design for reinforced adobe walls with geogrids), Pontificia Universidad Católica del Perú, Departamento de Ingeniería, Publicación DI-SIC-2009-01, Lima, Peru.

Torrealva, D., and Acero, J., 2005. Reinforcing adobe buildings with exterior compatible mesh: The final solution against the seismic vulnerability?, *SismoAdobe 2005: International Seminar on Architecture, Construction and Conservation of Earthen Buildings in Seismic Areas*, Lima, Peru.

U.S. Geological Survey (USGS), 2007. *ShakeMap 2007gbcv*, Published in http://earthquake.usgs.gov/earthquakes/shakemap/global/shake/2007gbcv.

Vargas, J., Blondet, M., Ginocchio, F., and Villa Garcia, G. 2005. 35 años de investigaciones en sismo adobe: La tierra armada (35 years of research on SeismicAdobe: Reinforced earth), *SismoAdobe 2005: International Seminar on Architecture, Construction and Conservation of Earthen Buildings in Seismic Areas*, Lima, Peru.

Vargas, J., Torrealva, D., and Blondet, M., 2007. *Building Hygienic and Earthquake-Resistant Adobe Houses using Geomesh Reinforcement for Arid Zones*, 1st edition, Pontificia Universidad Católica del Perú, Lima, Peru, 41 pp.

Zapata, I., and Torrealva, D., 2010. La Restauración de la Casa O´Higgins en Lima (Restoration of the O'Higgins House in Lima), *Congreso Internacional de Rehabilitación del Patrimonio Arquitectónico y Edificación CICOP 2010*, Centro de Extensión Pontificia Universidad Católica de Chile, Santiago, Chile.

(Received 29 October 2010; accepted 25 February 2012)